Check for updates

ADVANCED OPTICAL MATERIALS
www.advopticalmat.de

Squaraine Dyes for Single-Component Shortwave Infrared-Sensitive Photodiodes and Upconversion Photodetectors

Wei-Hsu Hu, Frank Nüesch, Davide Giavazzi, Mohammad Jafarpour, Roland Hany, and Michael Bauer*

Sensitive detection of shortwave infrared (SWIR) light using organic dyes will be a significant advance toward many applications in industry and research. Furthermore, from a fabrication and optimization view, photogeneration of charges in diodes consisting of a single dye layer will be highly attractive. However, SWIR dyes are scarce and organic photodiodes usually utilize a donor–acceptor materials combination to split excitons into charges. Here, it is demonstrated that single-component layers of several SWIR squaraine dyes operate as efficient photodetectors, with peak external quantum efficiency > 40% beyond 1000 nm and sensitivity out to 1300 nm. Photocurrents show a superlinear dependence on reverse bias. It is shown that this results from a field-assisted exciton dissociation mechanism, and not from field-dependent charge injection or extraction. SWIR photodiodes are combined with organic light-emitting diodes to fabricate upconversion photodetectors – devices that convert SWIR photons directly into visible light. Upconverters are characterized by a low turn-on voltage (1.5 V) and a high luminance contrast (on-off ratio 16 000) and SWIR-to-visible ($\lambda = 575$ nm) photon conversion efficiency (1.85%). Upconversion photodetectors emerge as a promising alternative to the current inorganic-based imaging technology.

1. Introduction

The growing interest in sensing and imaging of shortwave infrared (SWIR, $\lambda > 1000$ nm) light is related to the increasing number of applications in this spectral range, including biomedical imaging, optical communication, or machine vision systems.[1,2] To date, sensitive photodetection beyond 1000 nm is possible with inorganic semiconductor-based photodetectors and cameras. However, inorganic sensor arrays are rigid, require complex processing and are cost-prohibitive for low-end consumer applications.[3]

In this regard, organic materials can play a major role for photodetection in the SWIR. Organic photodetectors can be fabricated on flexible substrates, or can be deposited directly on complementary metal-oxide semiconductor readout circuits.[4] A few polymers with sensitivity extending into the SWIR have been synthesized.[5–7] Likewise, few organic dyes with peak absorption approaching the 1000 nm limit and beyond have been reported.[8–10] Most of these dyes belong to the families of cyanines,[11,12] charge-transfer dyes[13] or squaraines.[14] Among these, squaraine dyes have emerged as a large materials library for a wide variety of applications, including SWIR bioimaging and photodetection.[15,16]

Usually, efficient charge generation in organic materials can only be achieved by combining two materials to form a heterojunction, with one acting as the electron donor (D) and the other as the acceptor (A). In this case, photoexcitation forms an intermolecular charge transfer (CT) state, from which charge separation occurs.[17,18] A disadvantage of this approach is that the use of a two-component blend film introduces a large space for device optimization and morphological instabilities. Furthermore, because the optical gap for SWIR dyes is small, it gets increasingly difficult to find a suitable complementary component to form a D–A heterojunction.[5,7,19,20] There are a few reports on single-component organic solar cells where the D–A motif was combined in a single molecule or a co-polymer.[21] However, the synthesis of such molecules is difficult and the power conversion efficiencies were modest.

Therefore, it would be highly desirable to fabricate SWIR photosensitive organic devices from a single material, which offers the possibility for easy processing, morphological control and long-term stability. However, there are only few reports on

W.-H. Hu, F. Nüesch, M. Jafarpour, R. Hany, M. Bauer
Empa, Swiss Federal Laboratories for Materials Science and Technology
Laboratory for Functional Polymers
Dübendorf CH-8600, Switzerland
E-mail: roland.hany@empa.ch
W.-H. Hu, F. Nüesch, M. Jafarpour
Institute of Materials Science and Engineering
Ecole Polytechnique Fédérale de Lausanne, EPFL
Station 12, Lausanne CH-1015, Switzerland
D. Giavazzi
Dipartimento di Scienze Chimiche, della Vita e della Sostenibilità Ambientale
Università di Parma
Parco Area delle Scienze 17/A, Parma 43124, Italy

The ORCID identification number(s) for the author(s) of this article can be found under https://doi.org/10.1002/adom.202302105

DOI: 10.1002/adom.202302105

 © 2023 Wiley-VCH GmbH

intrinsic photocharge generation in the bulk of a single organic material, and photosensitivity was limited to the visible and near-infrared (NIR) out to ≈850 nm.[22–30] Intrinsic photoinduced charge generation for organic materials in the SWIR has not been reported so far.

For intrinsic charge generation in a single material to occur, the question is how the binding energy of the photogenerated exciton can be overcome. The driving force has been proposed to arise from energetic disorder in single-component films, because of energy level shifts due to electronic coupling between dye molecules and intermolecular electric fields.[22,23,30] Alternatively, and in some cases conjectural, an external electric field-assisted dissociation mechanism was postulated, or intrinsic charge generation was attributed to the high dielectric constant of the material, resulting in efficient charge screening and therefore allowing efficient electron-hole pair separation.

Recently, we investigated the synthesis and properties of the symmetrical benz[*cd*]indolium-capped squaraine dye (in this work named SQ1) and of the corresponding dicyanomethylene acceptor-substituted dye (DCSQ1). Using SQ1 and DCSQ1 as (D/A) dye/PCBM blend active layers, we demonstrated efficient photoinduced charge generation with peak sensitivity (1025 nm) in the SWIR.[31–33] Here, we extend the SWIR squaraine family and report on the synthesis of a benz[*cd*]indol-flanked, rhodanine-substituted dye (RSQ1) with an absorption maximum at 1072 nm.

For DCSQ1, SQ1 and RSQ1 we find that, unconventionally, efficient photoinduced charge generation occurs already in single-component photodiodes with an external quantum efficiency > 40%. Using a combination of experimental methods and simulations, we confirm that charge generation occurs in the bulk of the squaraine layers, and exclude that charges are injected from the external circuit or are primarily generated at an electrode/dye interface. Single-component diodes show superlinear (concave) dependence of photocurrent with reverse voltage. The superlinear photocurrent behavior is explained with an electric field-induced dissociation mechanism.

We then combine the single-component squaraine SWIR photodetectors with an organic visible light-emitting diode (OLED) to fabricate so-called upconversion photodetectors.[2] When SWIR light is absorbed in the photodetector, a current is generated and converted into a visible image by the OLED. Thereby, an upconversion photodetector directly converts SWIR light into visible light. The device concept needs no intermediate electronics for data processing, no external display for data visualization and allows high image resolution without pixelation of the active layer.[34,35] Upconversion photodetectors are also denoted as upconversion device[36] or upconversion imager/display[37–39] and are studied as an alternative to the current inorganic compound-based SWIR imaging technology. Our upconversion photodetectors convert SWIR photons up to 1300 nm directly into visible greenish-yellow photons, with good performance in terms of a low turn-on voltage, a high on-off ratio between the luminance measured in the presence of SWIR light and in the dark, as well as a high infrared-to-visible photon-to-photon conversion efficiency.

2. Results

2.1. Synthesis and Molecular Properties

For the synthesis of the RSQ1 squaraine, we replaced the dicyanomethylene group with the even stronger rhodanine acceptor (**Scheme 1**).[40] Experimental details for the RSQ1 synthesis are compiled in the Supporting Information. Scheme 1 also includes the chemical structures of the dyes SQ1 and DCSQ1. We used these dyes for the fabrication of single-component photodiodes in this work, and repeat in **Table 1** some structural and molecular properties from reference [31] for comparison purposes. The absorptions of SQ1 and DCSQ1 in solution (**Figure 1a**) are characterized by narrow peaks with high molar absorption coefficients far in the NIR range. For both dyes, absorptions between 300 and 400 nm are attributed to the absorption of the benz[*cd*]indole moiety. For DCSQ1, additional hypsochromic absorptions appear in the 450 nm – 600 nm range. These are assigned to higher energy transitions, which are symmetry-forbidden for SQ1 (C_{2h} symmetry) but weakly allowed for DCSQ1 (C_{2v} symmetry).[31]

Due to the steric demand of the rhodanine group, we assume for RSQ1 that the heterocycles on opposite sides of the polymethine chain arrange in a *cis* configuration, in accordance with DCSQ1. The rhodanine acceptor induces a substantial redshift of the absorption maximum to 1072 nm in solution. However, the bathochromic shift comes along with a broadening of the main absorption band and a strong decrease of the molar extinction coefficient (Table 1). At the same time, higher energy optical transitions in the visible become pronounced. The narrow absorption at 510 nm originates from the rhodanine squarate unit incorporated in RSQ1 (Figure S1, Supporting Information), additional allowed transitions with peak absorption at 635 nm are explained by the symmetry loss in RSQ1 due to the asymmetric rhodanine unit (Figure S2, Supporting Information).

Due to intermolecular interactions and increased molecular ordering, film absorbance spectra are considerably broadened compared to the solution spectra (Figure 1b–d; Figure S3, Supporting Information). For DCSQ1 and RSQ1, additional H-aggregate bands appear, suggesting that these dyes self-organize during film formation. Consistent with the peak absorption trend, the electrochemical gap narrows with increasing acceptor strength in the dye series (Table 1; and Figure S4, Supporting Information). The optical bandgaps from the onset absorption edge in solution differ from the electrochemical bandgaps by ≈0.07 eV for DCSQ1, and by ≈0.13 eV for SQ1 and RSQ1.

2.2. Single-Component Photodiodes

Photodiodes were fabricated as ITO/TiO_2 35 nm/dye 85 nm/MoO_3 15 nm/Ag 60 nm stack, with the squaraine dyes as single-component active layer, and TiO_2 and MoO_3 as electron- and hole-selective contacts, respectively. Figure 1b–d shows external quantum efficiency (EQE) spectra for these devices. At short-circuit (no external voltage applied), the EQE in the NIR/SWIR range was below 1% (Figure S5, Supporting Information), but EQEs increased strongly with reverse bias and reached 43% (at -10 V) or 13% (at -6 V) for DCSQ1 (at 1030 nm),

© 2023 Wiley-VCH GmbH

21951071, 0, Downloaded from https://onlinelibrary.wiley.com/doi/10.1002/adom.202302105 by Paul Scherrer Institut PSI, Wiley Online Library on [08/01/2024]. See the Terms and Conditions (https://onlinelibrary.wiley.com/terms-and-conditions) on Wiley Online Library for rules of use; OA articles are governed by the applicable Creative Commons License

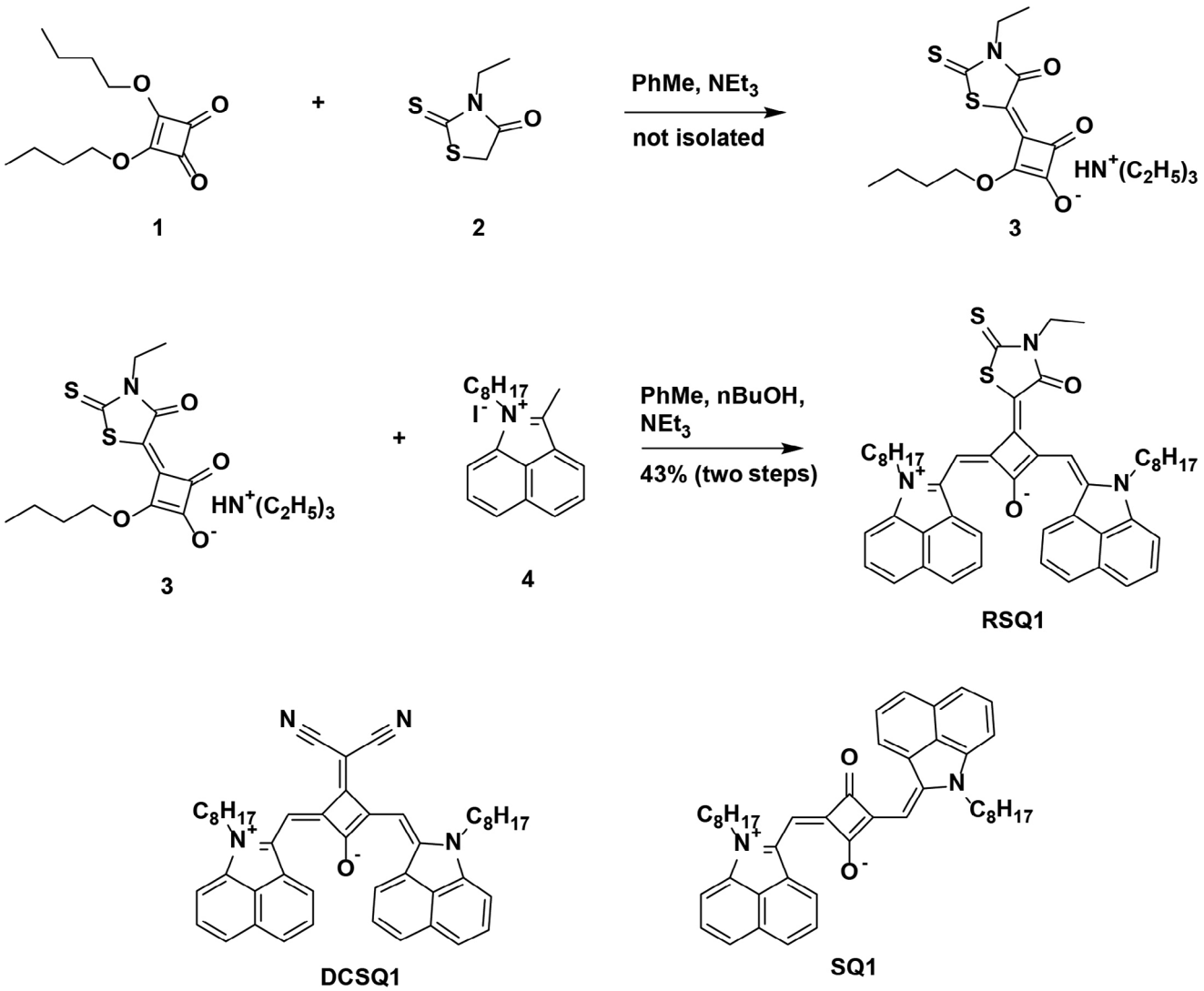

Scheme 1. Synthesis of the RSQ1 dye, which is composed of benz[*cd*]indole donor units and the rhodanine-substituted squarate acceptor unit. Included are the chemical structures of the recently synthesized dyes DCSQ1 and SQ1.[31]

and 30% for SQ1 (at -10 V, at 1015 nm). The RSQ1-based diode reached a maximum EQE of 7% (at 1140 nm) with increasing voltage applied, which we limited to a maximum of -6 V because of a rather high dark current and associated noisy EQE spectra for higher voltages. The high dark current is explained by the non-homogeneous film formation of RSQ1 on TiO_2 (Figure S6, Supporting Information). In the NIR/SWIR range, EQE spectra of all photodiodes follow the film absorbance spectra, and the RSQ1 device is sensitive out to a wavelength of 1300 nm (EQE = 1%). The apparent EQE peak at 450 nm in all spectra is

Table 1. Absorption and electrochemical data of squaraine dyes.

	Absorption				Cyclic Voltammetry			Reference
	$\lambda_{max,film}$ [a] [nm]	$\lambda_{max,sol.}$ [b] [nm]	ϵ [M^{-1} cm^{-1}]	$E_{gap,opt.}$ [c] [eV]	E_{HOMO} [d] [eV]	E_{LUMO} [eV]	$E_{gap,CV}$ [eV]	
SQ1	970	900	152 000	1.31	-5.14	-3.96	1.18	[31]
DCSQ1	995	958	137 000	1.21	-5.20	-4.06	1.14	[31]
RSQ1	1071	1072	25 500	1.03	-5.02	-4.12	0.90	this work

[a] Spin coated from chloroform solution onto a glass substrate [b] Measured in toluene [c] Optical gap from the absorption onset [d] Measured in CH_2Cl_2, potential against Fc/Fc^+, using −5.1 V eV for Fc/Fc^+ against vacuum.

© 2023 Wiley-VCH GmbH

21951071, 0, Downloaded from https://onlinelibrary.wiley.com/doi/10.1002/adom.202302105 by Paul Scherrer Institut PSI, Wiley Online Library on [08/01/2024]. See the Terms and Conditions (https://onlinelibrary.wiley.com/terms-and-conditions) on Wiley Online Library for rules of use; OA articles are governed by the applicable Creative Commons License

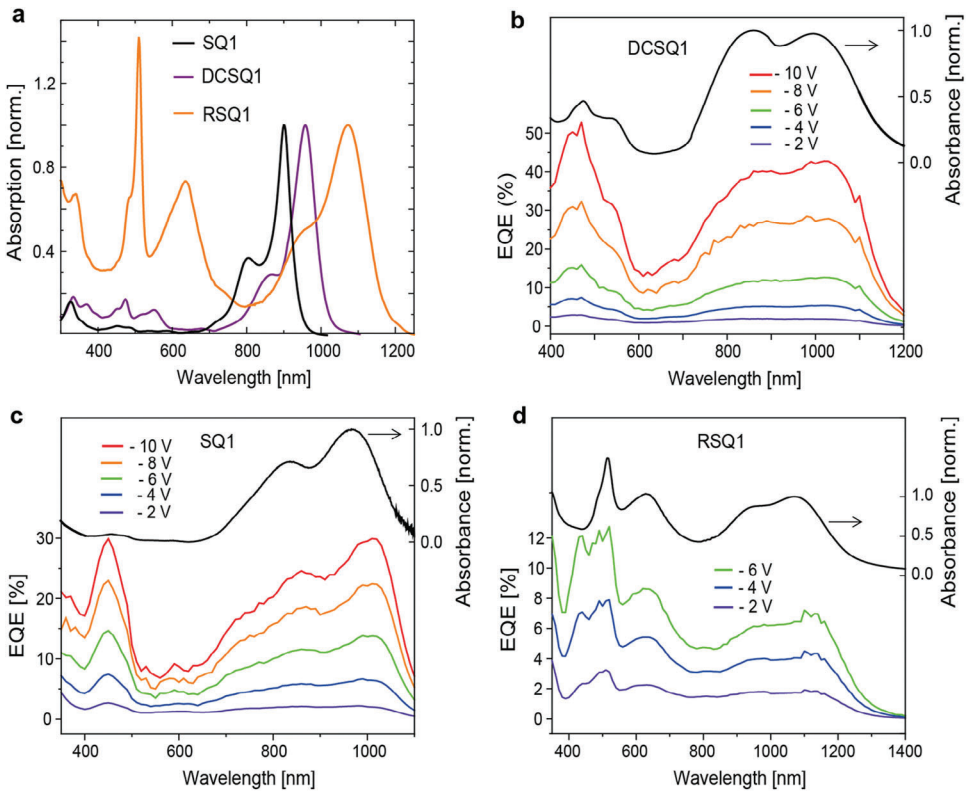

Figure 1. a) Absorption spectra of squaraines in toluene solution. b–d) EQE of single-component squaraine photodiodes as function of voltage bias (labeling EQE left y-axes). Dye film absorbance spectra are included (black color, labeling right y-axes); detailed spectra are shown in Figure S3 (Supporting Information).

ascribed to an optical interference effect (Figure S7, Supporting Information).[41]

We address two uncommon features from results shown in Figure 1. First, the outcome that quite efficient charge generation takes place after light absorption in single-component squaraine layers, second the result that EQEs depend strongly on the bias voltage. We concentrate the analysis on DCSQ1 because the associated photodiode performs best. **Figure** 2a shows EQE values extracted from Figure 1 and a current-voltage (J–V) trend of a DCSQ1 photodiode. These data indicate that the efficiency of photoinduced charge generation shows an onset voltage of ≈-2 V, after which the current density and EQE depend almost linearly on the reverse electric field. In order to confirm that charge generation occurs intrinsically in the bulk of the dye layers, it is necessary to verify that charges are not injected into the device from the external circuitry, as well as that charges are not mainly generated at a dye-electrode interface.

One mechanism to inject a large number of charges into the device is based on trap-assisted photomultiplication.[42,43] The effect occurs via tunneling-injection from one of the electrodes because of trapped photogenerated charges and charge injection depends exponentially on the applied field.[23] The superlinear electric field dependence of the photocurrent observed in our case is a strong indication that charge generation cannot be ascribed to external charge injection. Furthermore, because of slow trapping and detrapping of charges, photomultiplication type photodetectors usually show a slow response to a fast-switching light pulse.[42,44] Such a behavior is in contrast with results from transient photocurrent measurements (Figure 2b). For a DCSQ1 photodiode, the current rises and decays within less than 1 µs when a light pulse is applied. This is much faster than the response of trap-assisted photomultiplication photodetectors, which is in the order of milliseconds to seconds (Figure S8, Supporting Information).

We examine the possibility that charge generation occurs at a dye-electrode interface. Of importance is the TiO_2/dye interface, which is present in the so-called inverted device, ITO/TiO_2/dye/MoO_3/Ag. It is known that TiO_2 can be sensitized by direct electron transfer from a photoexcited dye into the TiO_2 conduction band, followed by regeneration of the dye ground state by hole transfer across MoO_3.[45,46]

This mechanism likely occurs in our photodiodes as well; however, charge generation in the bulk of the active materials prevails. Setting the exciton diffusion length in the dye film to a typical value of ≈5 nm,[47] we calculate that the percentage of absorbed photons within this dye layer thickness next to TiO_2 in the NIR/SWIR spectral region is below 10% (Figure S9, Supporting Information). This corresponds to a small fraction of the measured EQE of 43% at 1030 nm for DCSQ1. This calculation sets as an upper boundary that not more than ≈25% of the experimental photocurrent can be generated at the TiO_2/dye interface, which indicates that the majority of charges is generated in the bulk film. We support bulk charge generation by investigating diodes with a thick DCSQ1 layer, combined with a thin and

© 2023 Wiley-VCH GmbH

21951071, 0, Downloaded from https://onlinelibrary.wiley.com/doi/10.1002/adom.202302105 by Paul Scherrer Institut PSI, Wiley Online Library on [08/01/2024]. See the Terms and Conditions (https://onlinelibrary.wiley.com/terms-and-conditions) on Wiley Online Library for rules of use; OA articles are governed by the applicable Creative Commons License

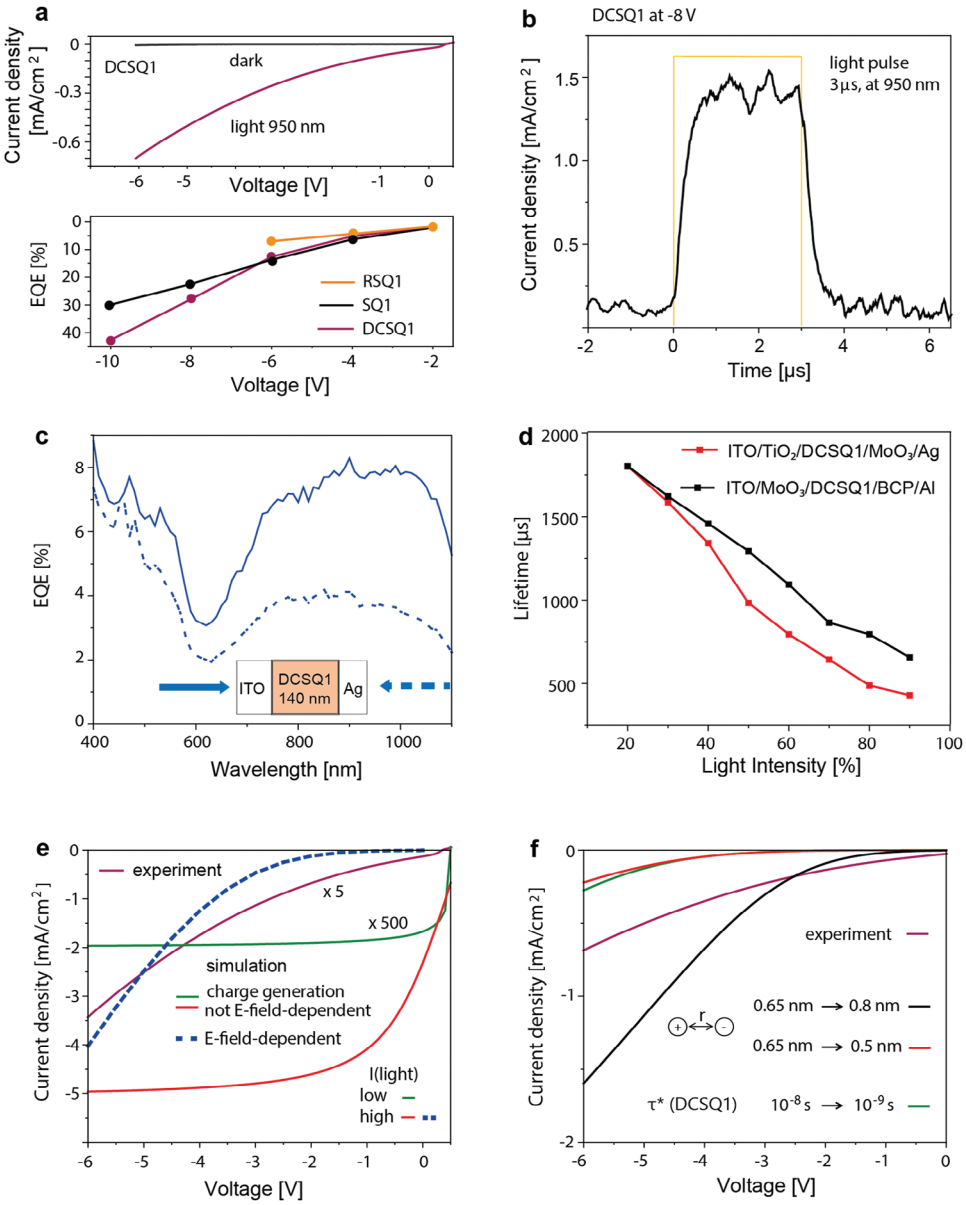

Figure 2. a) top: Current-voltage curves of a DCSQ1 photodiode in the dark and in the presence of NIR light. bottom: EQEs of squaraine photodiodes as function of the voltage bias (data from Figure 1). EQE data were taken at 1030 nm (for DCSQ1), at 1010 nm (for SQ1) and at 1140 nm (for RSQ1). b) Response of a DCSQ1 diode to a NIR light pulse. The current rise time (0% – 90%) was 0.5 µs, the fall time (100% – 10%) was 0.7 µs. The LED flux in (a, top) and b) was 1.2×10^{21} m^{-2} s^{-1}. c) EQE of an ITO/TiO_2/DCSQ1 140 nm/MoO_3/Ag 12 nm semitransparent photodiode at -10 V with light illuminated through the ITO (solid line) or the Ag (dotted line) side. d) Carrier lifetimes from transient photovoltage measurements for the regular and inverted device architecture. e) Simulation of the experimental current-voltage trend (data from Figure 2a) assuming electric field-assisted charge generation. f) Sensitivity of the simulation parameters τ^* (the lifetime of the excited state) and r (the electron-hole pair distance in the excited state).

semitransparent Ag layer, ITO/TiO_2/DCSQ1 140 nm/MoO_3/Ag 12 nm (Figure 2c). EQEs were measured with light incident through the ITO or the Ag side. At 1000 nm, the EQE was 7.8% for irradiation through ITO, and 3.5% when irradiating through Ag. We attribute this efficiency drop to incident light that is partially reflected at the semitransparent Ag electrode before entering the device. Assuming that charge-generation occurs mainly at the TiO_2/dye interface, the EQE would drop by a calculated factor of ≈10, much more than experimentally observed. This is because in this case most of the light from the Ag side would be absorbed in the thick dye layer before reaching the TiO_2 interface. This consideration is largely independent of the exact value of the exciton diffusion length (Figure S9, Supporting Information).

Furthermore, we fabricated diodes in the regular ITO/MoO_3/dye/BCP/Al architecture (BCP is bathocuproine), and found that the EQE was ≈25% smaller than for inverted devices (Figure S10, Supporting Information). In the regular device, the TiO_2 layer is not present at all. Again, this indicates that charge generation in both devices occurs predominantly in the bulk of the active layer, with a small fraction (≈25%) of

© 2023 Wiley-VCH GmbH

21951071, 0, Downloaded from https://onlinelibrary.wiley.com/doi/10.1002/adom.202302105 by Paul Scherrer Institut PSI, Wiley Online Library on [08/01/2024]. See the Terms and Conditions (https://onlinelibrary.wiley.com/terms-and-conditions) on Wiley Online Library for rules of use; OA articles are governed by the applicable Creative Commons License

charges generated in the inverted diode directly at the TiO_2/dye interface. This is finally consistent with results from transient photovoltage (TPV) measurements. During a TPV experiment, the device is kept at open-circuit. Therefore, no charges are injected from, or are extracted to, the external circuit, and all charges recombine inside the device, with the recombination time depending inversely on carrier concentration (Figure S11, Supporting Information). The extracted carrier lifetime for the regular device was slightly longer than for the inverted device (Figure 2d). This indicates that the number of generated charges in the inverted device was slightly larger, because of additional charge generation at the TiO_2/dye interface, which adds in the inverted photodiode to the charges generated in the bulk film.

We performed numerical simulations to investigate the superlinear EQE and current dependence on the electric field (Figure 2a). First, we assumed that photoexcitation generates charges with a certain probability (30% in our case) that is independent of the electric field. Simulation parameters are compiled in Table S1 (Supporting Information). *J–V* curves were simulated using a high or a low light intensity; these correspond to the experimental intensities used for the *J–V* and EQE measurements. In this case, simulated and experimental *J–V* trends do not match (Figure 2e). Simulated currents show a sublinear (convex) current versus voltage trend and reach a plateau at reverse bias, which indicates complete extraction of generated charges. For a low light intensity, charge recombination is insignificant and complete charge extraction occurs already at a small voltage of ≈ -1 V (Figure 2e, green curve). For the simulated high light intensity case, the current saturates at a slightly higher voltage of ≈ -3 V (Figure 2e, red curve).

A superlinear (concave) *J–V* trend emerges in the simulation if electric field-assisted charge generation is included (dotted blue line, Figure 2e). The simulation is based on the Onsager-Braun model[48] with an extension by Koster et al.[49] to include positional disorder of the initial electron-hole pair separation in the excited state (parameter r). The experimental current trend was simulated with r = 0.65 nm, the lifetime $\tau^* = 10$ ns of the excited state, and the experimental charge mobilities for electrons (μ_e) and holes (μ_h). Mobilities are field-dependent (Note S1, Supporting Information) and, e.g. at 3 V, $\mu_e = 1 \times 10^{-5}$ cm^2 V^{-1} s^{-1} and $\mu_h = 3 \times 10^{-6}$ cm^2 V^{-1} s^{-1}. With these parameters, the experimental *J–V* trend of a 40 nm thick DCSQ1 photodiode could be fitted as well (Figure S12, Supporting Information). Simulations in Figure 2f show that these parameters very sensitively affect the magnitude of the simulated current. For example, the current is much smaller for $\tau^* = 1$ ns (green curve) or r = 0.5 nm (red curve). On the other hand, the simulated current increases strongly for r = 0.8 nm (black curve). All simulated currents show that charge generation is activated only above a certain electric field strength (≈-2 V/85 nm in Figure 2e), after which it almost depends linearly on the field. Such a superlinear *J–V* trend is a characteristic signature of a field-assisted charge generation mechanism. The simulated current onset delay at reverse bias and the concave *J–V* trend is somewhat obscured in the experimental data, which we ascribe to the presence of the additional small current generated at the TiO_2/dye interface. This current is field-independent and superimposes with the field-assisted current.

2.3. Single-Component Upconversion Photodetectors

For the fabrication of upconversion photodetectors, we combined the single-component photodiodes with a single-component OLED (**Figure 3a**). The OLED is composed of a single layer of a thermally activated delayed fluorescence emitter material, CzDBA,[50] and ohmic electron and hole contacts are realized with a (MoO_3 6 nm/C_{60} 3 nm) anode and a (TPBi 4 nm/Al) cathode.[51] Both in the dark (no NIR light) and in the on-state (with NIR light), a voltage is applied. In the dark, TiO_2 blocks hole injection at the ITO and MoO_3 blocks electrons from flowing through the device. This suppresses the dark current, which is important to achieve a high luminance on/off ratio.

In the presence of NIR light, charges are generated in the DCSQ1 photodetector. Electrons are extracted via TiO_2 at the anode, and holes drift into the OLED where they recombine with injected electrons from the cathode under the emission of visible light (Figure 3b,c).

J–V and luminance versus voltage characteristics of the DCSQ1-based upconversion photodetector are shown in Figure 3d. The reproducibility of device fabrication is summarized in Figure S13 (Supporting Information), and corresponding data for an RSQ1-based upconversion photodetector are shown in Figure S14 (Supporting Information). The small dark current rise between 4 and 10 V (0.06 mA cm^{-2}) is accompanied by an increase of the dark luminance (≈1 cd m^{-2} at 10 V), which indicates that the dark current is composed of injected electrons and holes. We fabricated devices with an additional CBP electron-blocking layer; however, this did not further suppress the dark current (Figure S15, Supporting Information). In the presence of NIR light, device turn-on was consistently at ≈1.5 V (Figure S13, Supporting Information), and the luminance reached a value of ≈20 cd m^{-2} at 2 V. The maximum on/off ratio for the luminance was 16 000 at 4 V. In an upconversion photodetector, the current in the on-state is limited by the number of photogenerated holes in the photodetector and therefore is expected to saturate at high voltages. Because the EQE in our photodiodes strongly increases with voltage, we do not observe this expected current plateau, and the current and associated luminance increase continuously with increasing bias.

The current efficacy of the device was (28 ± 1) cd A^{-1}, independent of the voltage bias. The photon-to-photon conversion efficiency (P2PCE) describes the ratio between the visible emitted photons and the incident NIR photons. The P2PCE was 1.85% at 10 V (average (1.4 ± 0.3)% from 13 devices). The P2PCE can be approximated from the individual EQEs of the photodetector and the OLED (≈9%, Figure S16 (Supporting Information)). The EQE of the photodetector part is (10–15)% at an electric field of 10 V/active layer thickness. With this, the calculated efficiency is P2PCE ≈ EQE(photodetector) x EQE(OLED) = 0.13 × 0.09 = 1.2%, which is in agreement with the experimental result.

3. Discussion

The combination of the strong rhodanine acceptor with benz[*cd*]indolium donor groups afforded the RSQ1 dye with an absorption maximum at 1072 nm, which represents a substantial

© 2023 Wiley-VCH GmbH

21951071, 0, Downloaded from https://onlinelibrary.wiley.com/doi/10.1002/adom.202302105 by Paul Scherrer Institut PSI, Wiley Online Library on [08/01/2024]. See the Terms and Conditions (https://onlinelibrary.wiley.com/terms-and-conditions) on Wiley Online Library for rules of use; OA articles are governed by the applicable Creative Commons License

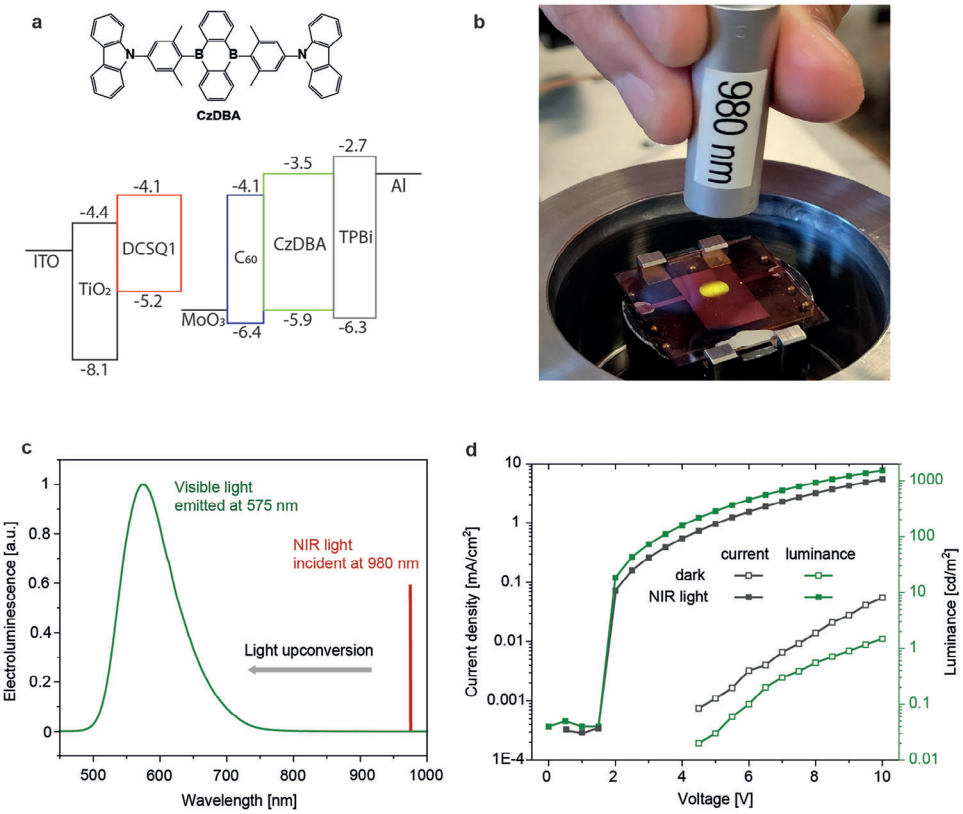

Figure 3. a) Upconversion photodetector stack, ITO/TiO_2 35 nm/DCSQ1 85 nm/MoO_3 6 nm/C_{60} 3 nm/ CzDBA 75 nm/TPBi 4 nm/Al 70 nm. CzDBA is 9,10-bis(4-(*9H*-carbazol-9-yl)−2,6-dimethylphenyl)−9,10-diboraanthracene, TPBi is 1,3,5-tris(*N*-phenylbenzimidazol-2-yl)benzene. b) Photo illustrating the upconversion process. A voltage bias (4 V) was applied to a rectangular (1 × 1.5 cm^2) device. The color of the device is violet. The device was irradiated with a NIR laser beam at 980 nm that has an elliptic form with semi-major axis lengths of 0.2 cm and 0.1 cm. The NIR light is upconverted to visible yellow light; this corresponds to the on-state. Because of the poor lateral conductivity and thin thickness of the organic layers, lateral current spreading in organic upconversion photodetectors is very small. Therefore, next to the NIR light beam no visible light is emitted, even though a voltage is applied; this corresponds to the dark, off-state. c) Electroluminescence spectrum of the visible emitted light. d) Performance characteristics of a DCSQ1 upconversion photodetector with and without NIR light (980 nm, 49 mW cm^{-2}). For better image contrast, the color of the emitted light in (c) and (d) is drawn in green; the actual emitted color in (b) is yellow.

bathochromic shift of 114 nm compared to the corresponding dicyanomethylene-based DCSQ1 dye (λ_{max} = 958 nm, Table 1). We assume that with stronger donor moieties more red-shifted rhodanine squaraines will be synthetically available. One successful donor motif was recently reported.[16] A dicyanomethylene squaraine with two diphenylamine-substituted benz[*cd*]indolium donor groups showed an absorption maximum at 1091 nm, which represents a bathochromic shift of 77 nm compared to the corresponding thienyl-substituted dye.[31] However, we reiterate that rhodanine is a chromophoric group and the resulting RSQ1 dye is non-symmetric and panchromatic. This is a problem if wavelength-selective SWIR sensing is required. It also presents a disadvantage for upconversion photodetector applications, because visible light that exits the device through the glass/ITO substrate is partially re-absorbed in the photodetector part. The same issues apply to many SWIR polymers that absorb also in the visible.[5–7,20]

We demonstrate efficient SWIR photoinduced charge generation in single-component squaraine two-terminal photodiodes. Further studies are required to judge whether these devices can find use as stand-alone high-performance photodetectors. A high EQE alone does not qualify the device as a practical photodetector, because this requires additional favorable performance metrics, such as a high linear dynamic range or a low dark/noise current (Note S2, Supporting Information).[8,10,45] However, when integrated in an upconversion device, a high EQE for converting SWIR photons into electrical charges is the essential requirement of the photodetector part. This is because in this case the device performance is governed by an intricate interplay between the photodetector and the OLED. For example, we showed recently that the response speed of an upconverter, namely the ability to accurately detect in the visible a rapidly changing infrared signal, is determined primarily by the electron mobility in the OLED,[46] and not by the response speed of the stand-alone photodetector.

Single-component photoinduced charge generation has been reported for a few other dyes before. For example, current generation in chloroboron subnaphthalocyanine was explained with direct carrier generation enabled by the materials high dielectric constant or by a field-assisted exciton dissociation mechanism.[26,29] Similarly, field-assisted charge generation was proposed for two (visible-absorbing) single-component

© 2023 Wiley-VCH GmbH

21951071, 0, Downloaded from https://onlinelibrary.wiley.com/doi/10.1002/adom.202302105 by Paul Scherrer Institut PSI, Wiley Online Library on [08/01/2024]. See the Terms and Conditions (https://onlinelibrary.wiley.com/terms-and-conditions) on Wiley Online Library for rules of use; OA articles are governed by the applicable Creative Commons License

squaraine photodetectors.[27,28] In our case, we derive field-assisted charge generation from the observation of a superlinear dependence of the photocurrent on reverse bias voltage, as well as from a detailed study to exclude that charges are injected into the device or are generated mainly at an electrode/dye interface. In reference, [23] a strong electric field-dependent photocurrent was explained with low and unbalanced mobilities for electrons and holes. From simulation, it was found that for balanced mobilities the current increases sublinear with voltage and reaches a plateau at reverse bias, but that a linear trend emerges for strongly imbalanced ($\mu_e/\mu_h < 0.05$) mobilities. In our photodiodes, this explanation does not apply. For DCSQ1, experimental charge mobilities are well balanced and do not differ by more than a factor 5 over the investigated voltage range. Furthermore, simulated curves based on imbalanced carrier mobilities over a sufficiently large negative voltage range always show a convex *J*–*V* trend (Figure S17, Supporting Information), which is opposite to the experiment (Figure 2).

We also measured the dielectric constants of the DCSQ1 film (Figure S18, Supporting Information). Typical dielectric constants for organic semiconductors at low frequency are in the range of 2.7 – 3.5.[52] In our case, the static dielectric constant up to several MHz is ϵ_{static} (DCSQ1) = 4.5, and the dielectric constant at optical frequencies is ϵ_{opt} (DCSQ1) = 3.8. These rather high dielectric constants favor intrinsic photocurrent generation, because they reduce all forms of charge recombination and space charge effects (ϵ_{static}) as well as reduce the exciton and (possibly) CT binding energy (ϵ_{opt}) in single-component squaraine films.[53–55]

The question whether the electric field splits the squaraine exciton directly or separates charges from a CT (excitonic) state[30] between neighboring, chemically identical squaraines moieties is not addressed in scope of this work. In principle, important information can be obtained from field-induced photoluminescence quenching studies.[30,56] However, this experiment is not possible with our fluorescence equipment because of the very low photoluminescence quantum yield (PLQY < 0.05% in solution[31]) of our squaraine dyes, which is likely due to the exponential increase of non-radiative losses when the energy gap decreases.[57]

Recently, intrinsic photogeneration in pristine cyanine films was explained with structural inhomogeneity creating energetic disorder.[22,23] Polymethine dyes (cyanines, squaraines) have a strong tendency to form aggregates, which coexist as nano-sized molecular ensembles with amorphous domains in the film.[58] Energy level variations arising from electronic coupling between aggregated molecules as well as local electric fields between amorphous and aggregated domains may shift the HOMO and LUMO energy levels.[22,59] Accordingly, a complex energetic landscape can emerge between different domains of chemically equivalent species, which possibly provides the driving force for exciton dissociation within the single-dye film, facilitated by the presence of an electric field in our case. As preliminary result, we observe that thermal annealing changes the squaraine films drastically from a mixed aggregate/amorphous to an aggregate-dominated morphology (Figure S19, Supporting Information). This mesoscale structural control over the dye arrangement is helpful to study mechanistic details of the intrinsic photoinduced charge generation in squaraines in future work.

4. Conclusion

In conclusion, we introduce the strong electron accepting rhodanine group to synthesize a SWIR squaraine dye with peak absorption (steadily) approaching the 1100 nm benchmark. We report that the rhodanine group is not suitable when selective spectral response in the SWIR range is required. In this regard, the synthetic challenge lies in the design of SWIR squaraine dyes using symmetric and visibly transparent acceptors, the dicyanomethylene group being a promising candidate.

We demonstrate efficient, electric field-assisted photocurrent generation in single-component squaraine photodiodes. The molecular structures of our squaraines and those used by others[27,28] for single-component photodiodes are markedly different. This raises the question whether intrinsic photocharge generation in squaraine films is driven by mesoscale structural inhomogeneity creating energetic disorder – as found for other organic materials[24] – or promoted by the efficient (field-assisted) dissociation of excitonic states linked to the intrinsic molecular D-A-D composition of this dye class.

We finally demonstrate efficient upconversion photodetectors. For SWIR-to-visible imaging applications with upconversion photodetectors, the availability of organic dyes with absorption beyond ≈1000 nm presents a crucial selling point. This is because upconverted light between ≈650 and 1000 nm, although not visible to the human eye, can also be detected with many digital cameras.

Supporting Information

Supporting Information is available from the Wiley Online Library or from the author.

Acknowledgements

Financial support by the Swiss National Science Foundation (grant IZBRZ2_186261), and from the Board of the Swiss Federal Institutes of Technology (grant SFA-AM SCALAR) is acknowledged. The authors thank Erwin Hack (Empa) for ellipsometry measurements, René Schneider (Empa) for optical microscopy measurements, Daniel Rentsch (Empa) for NMR measurements, and Anna Painelli and Cristina Sissa (University Parma, Italy) for helpful discussions.

Conflict of Interest

The authors declare no conflict of interest.

Data Availability Statement

The data that support the findings of this study are available in the supplementary material of this article.

Keywords

organic upconversion device, shortwave infrared, single-component photodetector, squaraine dye, upconversion photodetector

Received: September 15, 2023
Revised: November 30, 2023
Published online:

© 2023 Wiley-VCH GmbH

21951071, 0, Downloaded from https://onlinelibrary.wiley.com/doi/10.1002/adom.202302105 by Paul Scherrer Institut PSI, Wiley Online Library on [08/01/2024]. See the Terms and Conditions (https://onlinelibrary.wiley.com/terms-and-conditions) on Wiley Online Library for rules of use; OA articles are governed by the applicable Creative Commons License

[1] a) J. A. Carr, D. Franke, J. R. Caram, C. F. Perkinson, M. Saif, V. Askoxylakis, M. Datta, D. Fukumura, R. K. Jain, M. G. Bawendi, O. T. Bruns, *Proc. Natl. Acad. Sci. USA* **2018**, *115*, 4465; b) J. Zhao, D. Zhong, S. Zhou, *J. Mater. Chem. B* **2018**, *6*, 349; c) S. Zhu, R. Tian, A. L. Antaris, X. Chen, H. Dai, *Adv. Mater.* **2019**, *31*, 1900321.
[2] R. Hany, M. Cremona, K. Strassel, *Sci. Technol. Adv. Mater.* **2019**, *20*, 497.
[3] H. Ren, J.-D. Chen, Y.-Q. Li, J.-X. Tang, *Adv. Sci.* **2021**, *8*, 2002418.
[4] T. Rauch, M. Böberl, S. F. Tedde, J. Fürst, M. V. Kovalenko, G. Hesser, U. Lemmer, W. Heiss, O. Hayden, *Nat. Photonics* **2009**, *3*, 332.
[5] V. Yeddu, G. Seo, F. Cruciani, P. M. Beaujuge, D. Y. Kim, *ACS Photonics* **2019**, *6*, 2368.
[6] X. Gong, M. Tong, Y. Xia, W. Cai, J. S. Moon, Y. Cao, G. Yu, C.-L. Shieh, B. Nilsson, A. J. Heeger, *Science* **2009**, *325*, 1665.
[7] I. Park, C. Kim, R. Kim, N. Li, J. Lee, O. K. Kwon, B. Choi, T. N. Ng, D.-S. Leem, *Adv. Opt. Mater.* **2022**, *10*, 2200747.
[8] J. Huang, J. Lee, J. Vollbrecht, V. V. Brus, A. L. Dixon, D. X. Cao, Z. Zhu, Z. Du, H. Wang, K. Cho, G. C. Bazan, T.-Q. Nguyen, *Adv. Mater.* **2020**, *32*, 1906027.
[9] T. Weil, T. Vosch, J. Hofkens, K. Peneva, K. Müllen, *Angew. Chem., Int. Ed.* **2010**, *49*, 9068.
[10] T. Li, G. Hu, L. Tao, J. Jiang, J. Xin, Y. Li, W. Ma, L. Shen, Y. Fang, Y. Lin, *Sci. Adv.* **2023**, *9*, eadf6152.
[11] E. D. Cosco, J. R. Caram, O. T. Bruns, D. Franke, R. A. Day, E. P. Farr, M. G. Bawendi, E. M. Sletten, *Angew. Chem., Int. Ed.* **2017**, *56*, 13126.
[12] M. Young, J. Suddard-Bangsund, T. J. Patrick, N. Pajares, C. J. Traverse, M. C. Barr, S. Y. Lunt, R. R. Lunt, *Adv. Opt. Mater.* **2016**, *4*, 1028.
[13] G. Qian, B. Dai, M. Luo, D. Yu, J. Zhan, Z. Zhang, D. Ma, Z. Y. Wang, *Chem. Mater.* **2008**, *20*, 6208.
[14] U. Mayerhöffer, M. Gsänger, M. Stolte, B. Fimmel, F. Würthner, *Chem. - Eur. J.* **2013**, *19*, 218.
[15] a) K. Ilina, W. M. Maccuaig, M. Laramie, J. N. Jeouty, L. R. Mcnally, M. Henary, *Bioconjugate Chem.* **2020**, *31*, 194; b) J. He, Y. J. Jo, X. Sun, W. Qiao, J. Ok, T.-I. Kim, Z.' Li, *Adv. Funct. Mater.* **2021**, *31*, 2008201; c) J. H. Kim, A. Liess, M. Stolte, A.-M. Krause, V. Stepanenko, C. Zhong, D. Bialas, F. Spano, F. Würthner, *Adv. Mater.* **2021**, *33*, 2100582; d) D. Yao, Y. Wang, R. Zou, K. Bian, P. Liu, S. Shen, W. Yang, B. Zhang, D. Wang, *ACS Appl. Mater. Interfaces* **2020**, *12*, 4276.
[16] Y. Wang, M. Wang, G. Xia, Y. Yang, L. Si, H. Wang, H. Wang, *Chem. Commun.* **2023**, *59*, 3598.
[17] K. Vandewal, S. Mertens, J. Benduhn, Q. Liu, *J. Phys. Chem. Lett.* **2020**, *11*, 129.
[18] A. Devizis, A. Gelzinis, J. Chmeliov, M. Diethelm, L. Endriukaitis, D. Padula, R. Hany, *Adv. Funct. Mater.* **2021**, *31*, 2102000.
[19] Z. Wu, W. Yao, A. E. London, J. D. Azoulay, T. N. Ng, *Adv. Funct. Mater.* **2018**, *28*, 1800391.
[20] K. H. Hendriks, W. Li, M. M. Wienk, R. A. J. Janssen, *J. Am. Chem. Soc.* **2014**, *136*, 12130.
[21] a) S. Lucas, T. Leydecker, P. Samorì, E. Mena-Osteritz, P. Bäuerle, *Chem. Commun.* **2019**, *55*, 14202; b) S. Lucas, J. Kammerer, M. Pfannmöller, R. R. Schröder, Y. He, N. Li, C. J. Brabec, T. Leydecker, P. Samorì, T. Marszalek, W. Pisula, E. Mena-Osteritz, P. Bäuerle, *Sol. RRL* **2021**, *5*, 2000653; c) J. Roncali, I. Grosu, *Adv. Sci.* **2019**, *6*, 1801026.
[22] G. C. Fish, J. M. Moreno-Naranjo, A. Billion, D. Kratzert, E. Hack, I. Krossing, F. Nüesch, J.-E. Moser, *Phys. Chem. Chem. Phys.* **2021**, *23*, 23886.
[23] L. Wang, S. Jenatsch, B. Ruhstaller, C. Hinderling, D. Gesevicius, R. Hany, F. Nüesch, *Adv. Funct. Mater.* **2018**, *28*, 1705724.
[24] Y. Dong, V. C. Nikolis, F. Talnack, Y.-C. Chin, J. Benduhn, G. Londi, J. Kublitski, X. Zheng, S. C. B. Mannsfeld, D. Spoltore, L. Muccioli, J. Li, X. Blase, D. Beljonne, J.-S. Kim, A. A. Bakulin, G. D'avino, J. R. Durrant, K. Vandewal, *Nat. Commun.* **2020**, *11*, 4617.
[25] M. Wang, Y.-Z. Li, H.-C. Chen, C.-W. Liu, Y.-S. Chen, Y.-C. Lo, C.-S. Tsao, Y.-C. Huang, S.-W. Liu, K.-T. Wong, B. Hu, *Mater. Horiz.* **2020**, *7*, 1171.
[26] V. C. Nikolis, Y. Dong, J. Kublitski, J. Benduhn, X. Zheng, C. Huang, A. C. Yüzer, M. Ince, D. Spoltore, J. R. Durrant, A. A. Bakulin, K. Vandewal, *Adv. Energy Mater.* **2020**, *10*, 2002124.
[27] W. Li, D. Li, G. Dong, L. Duan, J. Sun, D. Zhang, L. Wang, *Laser Photonics Rev.* **2016**, *10*, 473.
[28] H. Guo, L. Jiang, K. Huang, R. Wang, S. Liu, Z. Li, X. Rong, G. Dong, *Org. Electron.* **2021**, *92*, 106122.
[29] H. T. Chandran, T.-W. Ng, Y. Foo, H.-W. Li, J. Qing, X.-K. Liu, C.-Y. Chan, F.-L. Wong, J. A. Zapien, S.-W. Tsang, M.-F. Lo, C.-S. Lee, *Adv. Mater.* **2017**, *29*, 1606909.
[30] S. Y. Park, C. Labanti, R. A. Pacalaj, T. H. Lee, Y. Dong, Y.-C. Chin, J. Luke, G. Ryu, D. Minami, S. Yun, J.-I. Park, F. Fang, K.-B. Park, J. R. Durrant, J.-S. Kim, *Adv. Mater.* **2023**, *35*, 2306655.
[31] K. Strassel, W.-H. Hu, S. Osbild, D. Padula, D. Rentsch, S. Yakunin, Y. Shynkarenko, M. Kovalenko, F. Nüesch, R. Hany, M. Bauer, *Sci. Technol. Adv. Mater.* **2021**, *22*, 194.
[32] K. Strassel, A. Kaiser, S. Jenatsch, A. C. Véron, S. B. Anantharaman, E. Hack, M. Diethelm, F. Nüesch, R. Aderne, C. Legnani, S. Yakunin, M. Cremona, R. Hany, *ACS Appl. Mater. Interfaces* **2018**, *10*, 11063.
[33] K. Strassel, S. P. Ramanandan, S. Abdolhosseinzadeh, M. Diethelm, F. Nüesch, R. Hany, *ACS Appl. Mater. Interfaces* **2019**, *11*, 23428.
[34] C.-J. Shih, Y.-Z. Li, M.-Z. Li, S. Biring, B.-C. Huang, C.-W. Liu, T.-H. Yeh, D. Luo, J.-H. Lee, Y.-H. Huang, K.-T. Wong, S.-W. Liu, *Nano Energy* **2021**, *86*, 106043.
[35] Z. He, X. Du, C. Zheng, X. Yu, H. Lin, S. Tao, *Adv. Sci.* **2023**, *10*, 2203870.
[36] a) D. Y. Kim, D. W. Song, N. Chopra, P. De Somer, F. So, *Adv. Mater.* **2010**, *22*, 2260; b) D. Yang, X. Zhou, D. Ma, A. Vadim, T. Ahamad, S. M. Alshehri, *Mater. Horiz.* **2018**, *5*, 874; c) N. Li, Z. Lan, Y. S. Lau, J. Xie, D. Zhao, F. Zhu, *Adv. Sci.* **2020**, *7*, 2000444; d) X. Du, J. Han, Z. He, C. Han, X. Wang, J. Wang, Y. Jiang, S. Tao, *Adv. Mater.* **2021**, *33*, 2102812; e) J. H. Kim, J.-Y. Lee, J. Lim, J. Roh, S.-W. Baek, W. Kim, M. C. Suh, H. Yu, *Adv. Funct. Mater.* **2023**, *33*, 2214530; f) Y. Zhang, Z. He, X. Du, J. Han, H. Lin, C. Zheng, J. Wang, G. Yang, S. Tao, *Opt. Express* **2022**, *30*, 16644; g) C.-J. Shih, Y.-C. Huang, T.-Y. Wang, C.-W. Yu, I.-S. Hsu, A. K. Akbar, J.-Y. Lin, S. Biring, J.-H. Lee, S.-W. Liu, *Sci. Adv.* **2023**, *9*, eadd7526.
[37] Q. Song, T. Lin, Z. Su, B. Chu, H. Yang, W. Li, C.-S. Lee, *J. Phys. Chem. Lett.* **2018**, *9*, 6818.
[38] N. Li, N. Eedugurala, D.-S. Leem, J. D. Azoulay, T. N. Ng, *Adv. Funct. Mater.* **2021**, *31*, 2100565.
[39] C. Shin, N. Li, B. Seo, N. Eedugurala, J. D. Azoulay, T. N. Ng, *Mater. Horiz.* **2022**, *9*, 2172.
[40] N. Terenti, G.-I. Giurgi, L. Szolga, I. Stroia, A. Terec, I. Grosu, A. P. Crișan, *Molecules* **2022**, *27*, 1229.
[41] M. Diethelm, Q. Grossmann, A. Schiller, E. Knapp, S. Jenatsch, M. Kawecki, F. Nüesch, R. Hany, *Adv. Opt. Mater.* **2019**, *7*, 1801278.
[42] L. Li, F. Zhang, W. Wang, Q. An, J. Wang, Q. Sun, M. Zhang, *ACS Appl. Mater. Interfaces* **2015**, *7*, 5890.
[43] H. Wei, Y. Fang, Y. Yuan, L. Shen, J. Huang, *Adv. Mater.* **2015**, *27*, 4975.
[44] J. W. Lee, D. Y. Kim, F. So, *Adv. Funct. Mater.* **2015**, *25*, 1233.
[45] H. Zhang, S. Jenatsch, J. De Jonghe, F. Nüesch, R. Steim, A. C. Véron, R. Hany, *Sci. Rep.* **2015**, *5*, 9439.
[46] W.-H. Hu, C. Vael, M. Diethelm, K. Strassel, S. B. Anantharaman, A. Aribia, M. Cremona, S. Jenatsch, F. Nüesch, R. Hany, *Adv. Opt. Mater.* **2022**, *10*, 2200695.
[47] O. V. Mikhnenko, P. W. M. Blom, T.-Q. Nguyen, *Energy Environ. Sci.* **2015**, *8*, 1867.
[48] C. L. Braun, *J. Chem. Phys.* **1984**, *80*, 4157.
[49] L. J. A. Koster, E. C. P. Smits, V. D. Mihailetchi, P. W. M. Blom, *Phys. Rev. B* **2005**, *72*, 085205.

© 2023 Wiley-VCH GmbH

21951071, 0, Downloaded from https://onlinelibrary.wiley.com/doi/10.1002/adom.202302105 by Paul Scherrer Institut PSI, Wiley Online Library on [08/01/2024]. See the Terms and Conditions (https://onlinelibrary.wiley.com/terms-and-conditions) on Wiley Online Library for rules of use; OA articles are governed by the applicable Creative Commons License

[50] T.-L. Wu, M.-J. Huang, C.-C. Lin, P.-Y. Huang, T.-Y. Chou, R.-W. Chen-Cheng, H.-W. Lin, R.-S. Liu, C.-H. Cheng, *Nat. Photonics* **2018**, *12*, 235.
[51] N. B. Kotadiya, P. W. M. Blom, G.-J. A. H. Wetzelaer, *Nat. Photonics* **2019**, *13*, 765.
[52] M. P. Hughes, K. D. Rosenthal, N. A. Ran, M. Seifrid, G. C. Bazan, T.-Q. Nguyen, *Adv. Funct. Mater.* **2018**, *28*, 1801542.
[53] Q. Lin, A. Armin, R. C. R. Nagiri, P. L. Burn, P. Meredith, *Nat. Photonics* **2015**, *9*, 106.
[54] P. Li, J. Fang, Y. Wang, S. Manzhos, L. Cai, Z. Song, Y. Li, T. Song, X. Wang, X. Guo, M. Zhang, D. Ma, B. Sun, *Angew. Chem., Int. Ed.* **2021**, *60*, 15054.
[55] A. Armin, D. M. Stoltzfus, J. E. Donaghey, A. J. Clulow, R. C. R. Nagiri, P. L. Burn, I. R. Gentle, P. Meredith, *J. Mater. Chem. C* **2017**, *5*, 3736.
[56] S. Tasch, G. Kranzelbinder, G. Leising, U. Scherf, *Phys. Rev. B* **1997**, *55*, 5079.
[57] R. Englman, J. Jortner, *Mol. Phys.* **1970**, *18*, 145.
[58] J. H. Kim, T. Schembri, D. Bialas, M. Stolte, F. Würthner, *Adv. Mater.* **2021**, *34*, 2104678.
[59] J. R. Lenhard, B. R. Hein, *J. Phys. Chem.* **1996**, *100*, 17287.

© 2023 Wiley-VCH GmbH

21951071, 0, Downloaded from https://onlinelibrary.wiley.com/doi/10.1002/adom.202302105 by Paul Scherrer Institut PSI, Wiley Online Library on [08/01/2024]. See the Terms and Conditions (https://onlinelibrary.wiley.com/terms-and-conditions) on Wiley Online Library for rules of use; OA articles are governed by the applicable Creative Commons License